1

Organic Crystalline Nanofibers

H.-G. Rubahn

Summary. Organic crystalline nanofibers are a new class of nanoscaled organic materials that bear high potential as model systems for optics and photonics at the diffraction limit. In addition, due to the possibility to tailor to a large extent morphology as well as optoelectronic properties, organic nanofibers are promising elements for future integrated devices. In this chapter the specific growth conditions are discussed that make the fabrication of this kind of matter possible as well as a range of applications in nano- and microoptics.

1.1 Introduction

Nanooptics is about understanding and mastering the interface between the micro- and the macroworld using optical methods. In doing so new optical properties are found which are based on the dimensional confinement that is a characteristic of nanoscaled materials. Metallic "quantum dots" such as Au nanoclusters are a good example of this domain, where changes in the size of the objects result in drastic changes of the optical properties [1]. These quantum dots have been well-studied in order to understand the fundamentals of the optoelectronic response in the nanodomain. In the meantime, they are also already used for, e.g., enhancing the brightness and stability of fluorophores for biological imaging and are as such commercially available [2]. This illustrates the speed with which basic research results transfer into industrial products in this field.

Another example – now based on dielectric materials – is photonic band gap (PBG) materials [3]. Here, a periodic index modulation is manufactured in dielectric slabs (e.g., by laser- or electron-beam-drilling a matrix of submicron-sized holes) which in the following inhibits the propagation of light of certain colors over a large range of scattering angles. In analogy to solid state physics this is called an "optical band structure." Again, the commercialization occurred on the very short time scale of a few years, and optical fibers implementing the PBG effect are now available for a wide range of applications [4]. In contrast to the above-mentioned quantum dots the PBG effect

can be quantitatively understood using classical electrodynamics. And indeed the possibility to model the optical behavior of submicron-scaled materials using classical methods is often encountered in the context of nanooptics.

The above examples from metallic and dielectric nanoscaled systems should not give the impression that optics in the subwavelength size regime is well understood. The influence of morphological changes on a nanometer-scale on the optical near field and from that on the resulting far field needs to be as well investigated as the corresponding influence on the spectroscopic properties, the waveguiding or the intrinsic dynamics of optical excitations in nanoaggregates. On the application side, a thorough understanding of morphology dependencies is an important prerequisite for the controlled build-up of new nanoscaled optoelectronic elements such as light emitting devices or field effect transistors.

In this chapter we describe generation and control of *organic crystalline* nanofibers, which constitute a recently developed model system that bears a high application potential. Using organic molecules instead of inorganic compounds to build up nanostructures has the advantage of being able to work with higher luminescence efficiency per material density, higher flexibility in terms of spectroscopic properties as well as easier and cheaper processing since controlled self assembled growth can be implemented.

This chapter begins with a discussion of the growth of ultrathin organic films on well defined, single crystalline substrates. It will be shown that the growth in general depends on both molecular parameters such as chain length as well as substrate parameters such as surface free energy, polarity, roughness, etc. Depending on the exact growth conditions such as substrate temperature or growth rate, films can be generated that consist of molecules with different orientations with respect to the surface normal, namely nearly parallel ("upright") or perpendicular ("laying"). Further optimization of the growth conditions results in the generation of needle-like but nonoriented structures on alkali halide crystals. Finally, by the use of the most appropriate substrate and fully optimized growth parameters, either dense arrays of nanofibers or isolated nanofibers are grown. Once this has been achieved, the substrate surface serves mainly as a template for producing tailored nanoaggregates, which in a next step are transferred onto other substrate surfaces.

1.2 Growth of Ultrathin Films: Molecular Orientation Control

In the past, various light emitting organic molecules have been investigated in terms of their abilities to form well-organized, ultrathin films for applications in optics or organic electronics [5]. Among those are thiophenes [6], PTCDA [7], pentacene [8], *para*-phenylenes [9], or anthraquinone [10] (Fig. 1.1). Up to now *para*-phenylenes have been found to provide us with the most

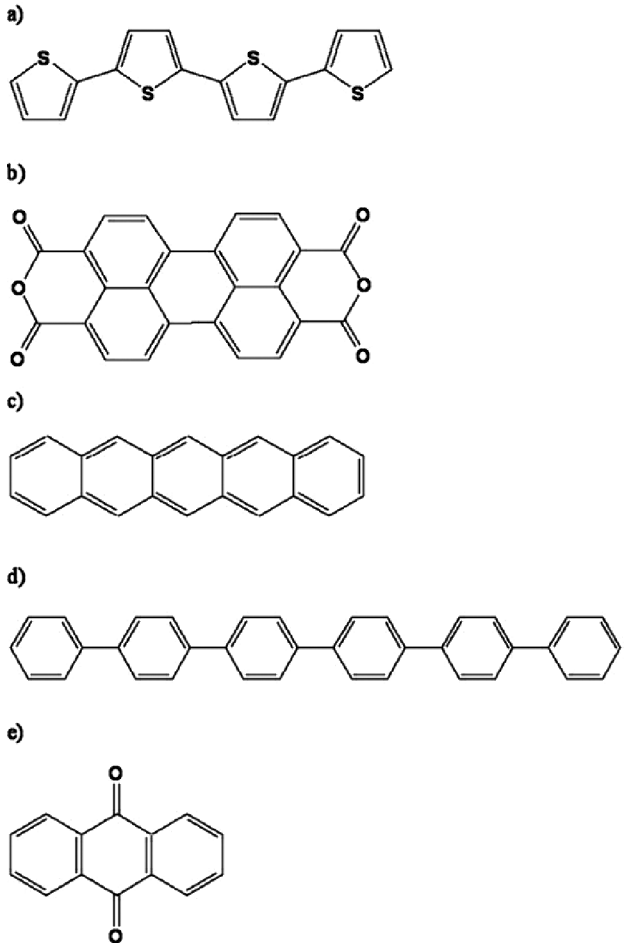

Fig. 1.1. Some organic molecules that have been used for building up ultrathin light-emitting films or nanostructures are **a**, α-4T; **b**, PTCDA; **c**, pentacene; **d**, *para*-hexaphenylene; **e**, anthraquinone

promising nanoaggregates, and therefore we will concentrate here on this class of molecules.

The short-chain *para*-phenylenes (*p*-nP, $n = 4$–6) form semiconducting films or aggregates with rather delocalized π-electrons, and they emit blue light after excitation with either UV light (around 360 nm) or electrons. Films of this material have attracted a great deal of attention over the last years [11]. Because of their promising chemical and optical properties [12–14] they are well-suited candidates for building up active layers in organic light-emitting diodes (OLEDs) [15, 16], organic field effect transistors (OFETs) [17], and other electronic and optoelectronic devices [18].

In principle, the molecules might be oriented either normal to the substrate or they might be aligned parallel to the substrate surface. The orientation has a strong influence on the device properties of the resulting films or nanoaggregates. For example, the electrical conductivity for *p*-6P is highest perpendicularly to the molecules long axes since the HOMO has highest electron density near the middle of the molecule. As a result, films of oriented molecules conduct also better in the direction perpendicular to the molecular axes [19]. Therefore one needs to characterize and optimize the molecular orientation. The characterization is rather simple in the case of a single crystalline film with large domains since the individual molecules possess a well-defined orientation with respect to the surface plane. In addition the main optical transition dipole moment is usually oriented along the long axes of the molecules and thus polarized absorption and emission studies can reveal the molecular orientations. For example, if all the molecules are oriented upright on the surface, then excitation under normal incidence will not result in light absorption and thus also not in luminescence.

Figure 1.2 demonstrates that characteristic features in the absorption spectra allow one to distinguish between upright and laying molecules. A pronounced absorption maximum at 280 nm characterizes upright molecules. The position of this maximum is independent of the substrate material. A maximum at 340 nm characterizes laying molecules. Both maxima shift with chain length of the molecules to the red spectral regime, in agreement with theoretical predictions [20]. Another way to determine the orientation of the molecules is atomic force microscopy (AFM). Examples for a continuous film of upright oriented *p*-4P molecules and a part of a needle-like structures ("nanofiber," see later) made of laying *p*-6P molecules are shown in Figs. 1.3a, b. Height scans indicate in the case of the continuous film terraces with height distances that correspond to tilted, normal oriented molecules (1.8 nm effective length). For the nanofiber (Fig. 1.3b) no domains with characteristic corrugation of 2.5 nm (the length of a normal oriented and tilted *p*-6P molecule) are found. These conclusions agree with local optical measurements.

In order to obtain well-defined single crystalline organic films on dielectric substrates subtle deposition control is needed. We have used a high vacuum system (base pressure 10^{-9} mbar) equipped with a fast entry lock and a multi-channelplate low energy electron diffraction spectrometer for the deposition of organic molecules and characterization of the resulting films. Muscovite mica and alkali halide single crystals were cleaved in air, transferred into the apparatus, and were outgassed thoroughly at temperatures around 370 K. The substrates could be heated by a tungsten filament, and deposition took place at substrate temperatures between room temperature and 420 K via sublimation of the organic compounds from a Knudsen cell. Deposition rate and final thickness of the organic films were controlled via a gold-plated and water-cooled quartz microbalance. Following deposition, LEED patterns were recorded in situ to verify the growth of single crystalline films or nanoaggregates. Depending on deposition rate, substrate type, and substrate

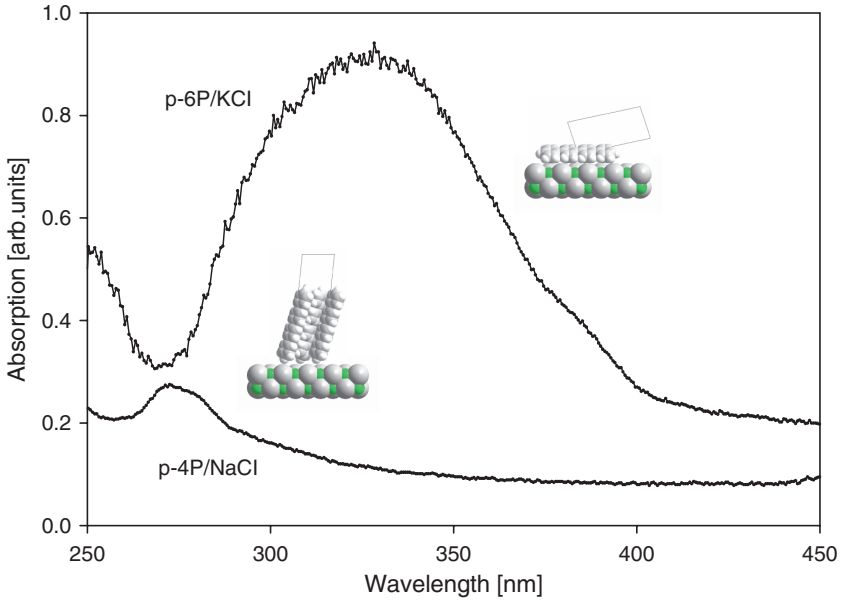

Fig. 1.2. Measured absorption spectra for films of upright oriented *p*-4P molecules on NaCl and laying *p*-6P molecules on KCl. The absorption is given in arbitrary units and thus not to be mutually compared

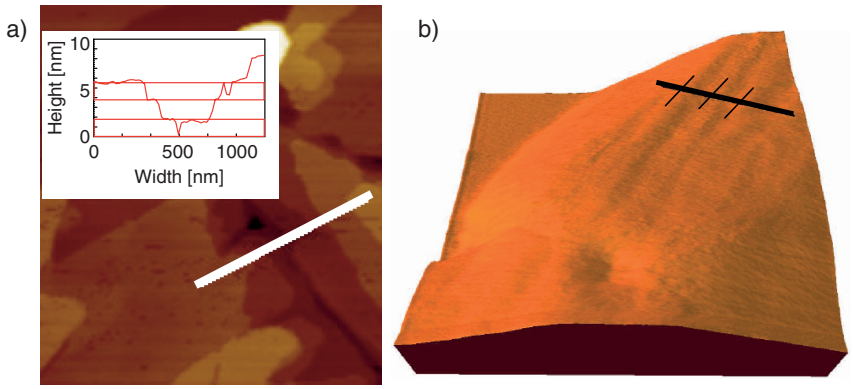

Fig. 1.3. (**a**) AFM image ($2.17 \times 2.17\,\mu m^2$) of a film of standing *p*-4P molecules on lithium fluoride. Height information is given as a linescan in the inset. (**b**) Same as (**a**) but an AFM image ($0.4 \times 0.4\,\mu m^2$) of a part of a nanofiber on mica (height scale 30 nm). We observe a modulation with 30 nm periodicity (*black lines*) which is due to the crystalline phase of the aggregates and not correlated to height variations due to individual molecules

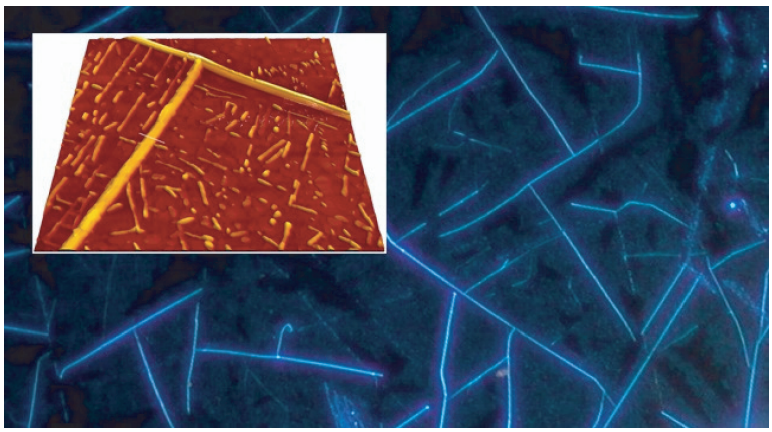

Fig. 1.4. Needle film of *p*-5P on NaCl, generated at surface temperature of 330 K. The inset is an AFM image ($6.5 \times 6.5\,\mu m^2$)

temperature, films with molecules oriented normal or parallel to the surface can be obtained.

For example, if one adsorbs *para*-phenylenes at high deposition rates ($0.5\,nm\,s^{-1}$) films of molecules oriented parallel to the surface are found in general [21]. At low deposition rates ($0.02\,nm\,s^{-1}$) the molecules are oriented normal to alkali halide surfaces if the deposition is performed at high temperatures. At room temperature films of parallel oriented molecules are generated on alkali halides, whereas on mica molecules are oriented normal to the surface. If one modifies the mica surface by, e.g., rinsing it in water or methanol, then a wetting layer of normal oriented molecules is generated even at high temperatures and at low deposition rates [22].

A closer look at the alkali halides (Fig. 1.4) shows that in addition to a continuous film of *p*-5P molecules needle-like aggregates can be generated. The needles have widths of the order of a few hundred nanometers and heights of the order of a few ten nanometers. They are statistically distributed over the surface. Similar needle growth is observed on other surfaces such as TiO_2, too [23]. Since the needles show waveguiding properties we will use the term *nanofibers* as an acronym.

1.3 Needle Films on Dedicated Templates: Mutual Orientation and Morphology Control of Nanoaggregates

1.3.1 Plain Mica

Under certain growth conditions *oriented* needle growth is observed on muscovite mica surfaces (Fig. 1.5) [24, 25]. Whereas height and width of the needles are similar to those found on alkali halides, they are much longer

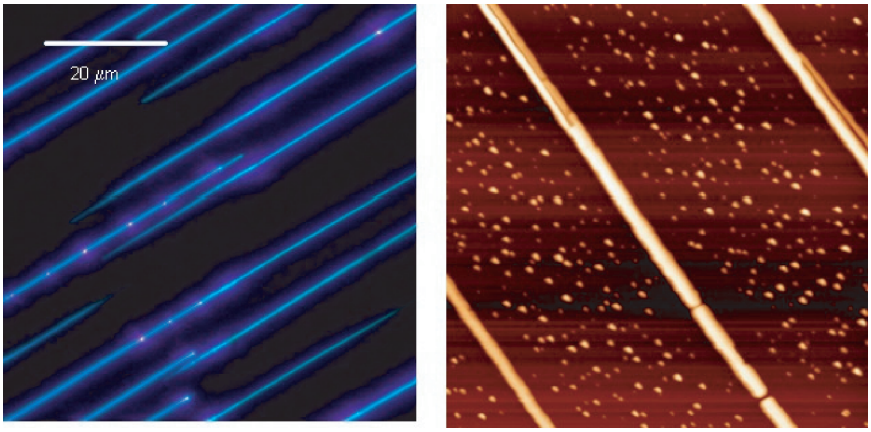

Fig. 1.5. Hexaphenyl nanofibers on mica, generated at a surface temperature of 400 K. *Left-hand-side*: epifluorescence image. *Right-hand-side*: AFM image ($6.4 \times 6.4\,\mu m^2$, height scale 80 nm)

(up to several hundred micrometers) and they are very well mutually oriented. Detailed investigations via electron diffraction and using optical methods have shown that the growth mechanism of the needles is influenced by strong electric dipole fields that are induced on the mica surface upon cleavage [25]. These dipole fields possess two possible orientations on a cleavage plane of mica (three, if one takes into account lower lying planes), and they do not exist on alkali halide surfaces. The dipole fields induce a dipole moment in the polarizable organic molecules, leading to an attraction via dipole-induced dipole forces and thus to an alignment of the individual organic molecules along the surface dipole orientations. Subsequent molecules grow side-by-side on the adsorbed molecules on the mica surface if they possess enough surface mobility (i.e., if the surface is warm enough), leading to the generation of aligned, needle-like aggregates with very well-defined molecular orientations.

The needle growth process is thus dictated by the strength and orientation of the dipole fields on the surface, the polarisability of the molecules and their mobility on the surface. Domains with specific dipole directions can be huge on mica (of the order of square millimeters to centimeters) and consequently huge domains with parallel oriented nanoaggregates can be formed. The temperature window for the growth of long needles within which the surface has to be kept is only of the order of 20–30 K; at lower temperatures quasicontinuous films consisting of very short, dense needles are formed. This strong temperature dependence allows one to grow the needles at predefined spots on the surface via, e.g., local laser heating [26], and enables control over the environment of individual needles. In other words, large areas with equally distributed needles of the same morphology can be generated, but also

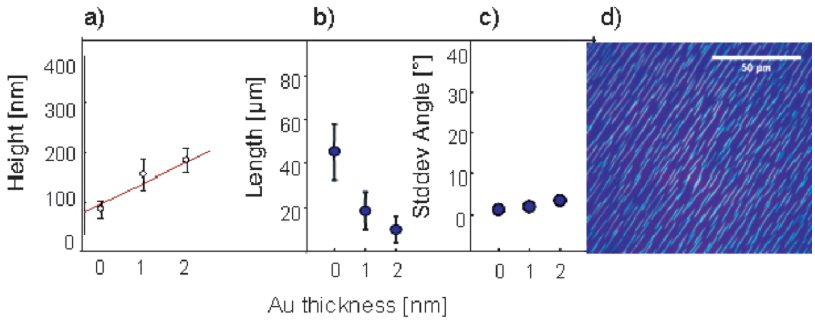

Fig. 1.6. Influence of an ultrathin Au film on the morphology (height (**a**), length (**b**)), and orientation (**c**) of *para*-hexaphenyl nanofibers on mica. (**d**) Epifluorescence image of the sample with 2 nm Au [27]

areas that contain just a few, uniquely identifiable needles. Both extremes are interesting in terms of fundamental nanooptical studies.

1.3.2 Au-Modified Mica

Besides control over mutual orientations and density, control over the morphology of individual nanoaggregates is also important. In general it is found that height and width of the nanoaggregates can be set rather independent of each other, i.e., needles of constant height but with variable width can be generated by adjusting the growth conditions on plain mica surfaces. However, one usually pays for this variability with a very wide length distribution.

More controllable results are obtained by modification of the mica surface before starting the organic film growth with, e.g., an ultrathin film of gold nanoclusters. Figure 1.6 demonstrates the influence of such a layer on the morphology and orientation of *p*-6P nanofibers. The plotted height has been determined by atomic force microscopy, whereas length and mutual orientation have been determined with the help of epifluorescence microscopy. As seen, increasing the Au thickness results in a drastic decrease of lengths of the nanofibers as well as a significant increase in heights. The degree of mutual orientation of the nanofibers, however, described via the standard deviation from a global orientation angle with respect to the substrate orientation does degrade only weakly.

If one further increases the Au thickness to 5 nm, this behavior changes drastically, the spread in orientation angle increases to 40° and the length decreases to a few micrometers. Thus especially the slight modification with a very thin film leads to the most useful results. It is also noted that the overall luminescence efficiency of the needle film depends on the Au cluster decoration. With increasing Au film thickness the luminescence first decreases, but then for film thicknesses larger than 5 nm it increases again and becomes even stronger than the luminescence without Au decoration [27]. Apparently

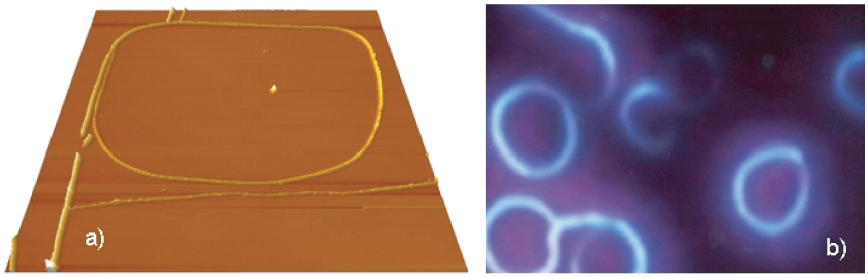

Fig. 1.7. Bent organic nanofibers (p-6P) on hydrophilized mica: (**a**) AFM image ($60 \times 60\,\mu m^2$, height scale 150 nm) and (**b**) epifluorescence image ($17.5 \times 25\,\mu m^2$). Each ring in the optical image has a diameter between 4 and 5 µm and wall widths of the order of 100 nm [22]

the Au film acts as a rough mirror and channels the emitted light along the surface normal.

1.3.3 Water-Treated Mica

As demonstrated before, a strong modification of the mica surface with, e.g., a Au cluster film results in less straight nanofibers. However, we do not observe significantly bent nanoaggregates such as rings. Ring-formation occurs if one rinses the mica surface before organic film growth with water and thus changes the surface hydrophobicity. In that case curved needles and rings or bent organic nanofibers of various sizes are observed (Fig. 1.7). AFM images reveal that these structures grow on a wetting layer of upright oriented molecules and that the height to width ratio is different from that found for straight needles [22]. Typical rings have widths of around 100 nm, i.e., smaller than that of the straight needles at similar growth conditions (around 300 nm), but they are significantly higher (a few hundred nanometers). Especially the circular rings show rather narrow size distributions. Optical measurements reveal that the molecules making up the rings are oriented radially, i.e., the rings are truly bent nanofibers.

Following achievement of a high degree of growth control, the nanofibers are used for investigating optical pecularities in the nanodomain. In the following, various applications are only briefly discussed. For a more complete description the reader is referred to the original literature.

1.4 Selected Applications in Nano- and Microoptics

Light emitting nanofibers are an interesting model system for demonstrating the resolution limit of optical microscopy at the interface between micro- and macrocosmos. In Fig. 1.8 dark field and epifluorescence images of the same hexaphenyl nanofiber are shown. Structures with characteristic dimensions of

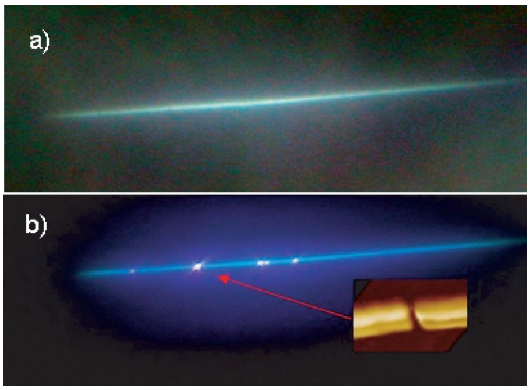

Fig. 1.8. Comparison of dark field (**a**) and epifluorescence (**b**) images of the same nanofiber. The inset is an AFM image ($1 \times 1.5\,\mu m^2$, height scale 60 nm) of a break in the nanofiber that gives rise to a bright luminescence spot

a few ten nanometers such as breaks in the nanofibers (exemplified by an AFM image in Fig. 1.8b) are barely visible even in dark field images since the difference in indices of refraction of nanofibers and underlying substrate is small. In dark field microscopy (Fig. 1.8a) one illuminates the sample under nearly grazing incidence, thus enhancing the visibility for structures on the surface that scatter light. Consequently such structures appear bright on a dark background. Note that the structures seen in Fig. 1.8 have heights of less than 100 nm, i.e., much smaller than the wavelength of the light used for scattering.

Much better contrast and visibility of subwavelength structures is obtained in epi-fluorescence microscopy (Fig. 1.8b). In such a set up UV light irradiates the nanofibers under normal incidence and the resulting luminescence is observed under normal incidence, too. Excitation and luminescence light are separated with the help of a wavelength selective beam splitter and color filters. At the breaks in the needles the internally generated luminescence is scattered into the far-field and thus submicron structures become easily visible. The true dimensions of the breaks, of course, cannot be determined via optical far field microscopy.

The possibility to separate the nanofibers widely from each other (i.e., with distances that are larger than the wavelength of the emitted light) as well as their macroscopic long axes allow one to investigate in detail the influence of morphological changes in the nanometer-range on the optical properties. As an example we show in Fig. 1.9 spectra obtained from a single nanofiber (circles) and from an ensemble of nanofibers (solid line). The spectrum from the single nanofiber has been obtained by illuminating the nanofiber inside a microscope with UV light and sampling the emitted light also inside the microscope with an optical fiber, connected to a miniature spectrometer. The relatively sharp spectral lines (given that the light is emitted from organic aggregates and that the samples are hold at room temperature) are due to a vibronic progression

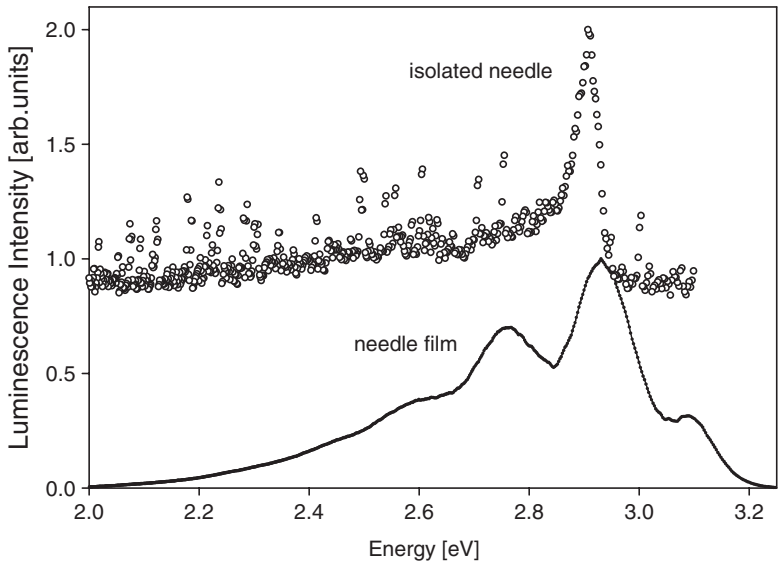

Fig. 1.9. Room temperature luminescence spectra obtained from an isolated nanofiber (*open circles*) and an ensemble of nanofibers (*solid line*). The equidistant lines on top of the graph represent the expected vibronic progression due to the C-C stretching vibrations of all carbon atoms of the individual molecules in the nanofiber. Due to reabsorption the highest energy (0-0) mode is relatively weak. It becomes stronger if one cools the sample [28]

of the exciton emission (perpendicular lines on top of the graph). In the case of the single nanofiber spectrum the highest energy (0,0) band is not visible due to a cut-off-filter in the microscope. Nevertheless, comparison with the spectra from the needle ensembles reveals that the light emission becomes more focussed to a narrow color range (namely $420 \pm 5\,\mathrm{nm}$) if an individual nanoaggregate is considered. More extended spectroscopic measurements along a nanofiber show that the spectral width of this residual line depends on the morphology of the aggregate and that it becomes narrower if the nanofiber width decreases, e.g., at the tip of the nanofiber [28].

If one increases the intensity of the excitation light, nonlinear optical effects can be observed in the nanofibers. The collective nonlinear optical response of oriented arrays of *para*-hexaphenylene nanofibers has been studied using femtosecond laser pulses [29]. At excitation wavelengths between 770 and 786 nm contributions to the two-photon signal intensity from both two-photon luminescence (TPL) and second harmonic generation (SHG) have been observed, where $I_{\mathrm{SHG}}/I_{\mathrm{TPL}} \approx 0.015$. More recent studies of SHG from nanofibers transferred onto glass substrates have shown that the SHG signal observed in [29] must have resulted from the wetting layer on the mica substrate. If one modifies *para*-quaterphenylene by adding electron donor and acceptor groups (e.g., methoxy- and amino-groups) and grows nanofibers from these functionalized

molecules, then the increased hyperpolarizability of the molecules results in strong SHG from the nanofibers [30].

The next logical step is to use the nonlinear optical signal to obtain spatially resolved information on molecular properties of the nanoaggregates. By use of a two-photon microscope the *local* polarized two-photon intensity along individual *p*-6P nanofibers could be determined [31]. Figure 1.10 shows polarized $10\times10\,\mu m^2$ two-photon images of nanofibers on mica. The nanofibers were excited again with a femtosecond laser at 780 nm. From a comparison of the intensity distributions at different polarization directions and employing the tensorial nature of the respective optical response one can deduce local orientations of the hexaphenyl molecules along the nanofibers. Essentially, just as in the linear case the absorption (and luminescence) is maximum if the electric field vector is parallel to the long molecular axis (which in turn is parallel to the optical transition dipole moment) and minimum if it is oriented perpendicular to it.

Using the two-photon luminescence instead of the one-photon luminescence increases the spatial resolution and the signal-to-noise-ratio of the method. That way for all of the nanofibers shown in Fig. 1.10 molecular orientations could be determined with a spatial resolution of less than 1 µm [31]. The results agree with possible molecular orientations predicted from bulk growth of a *para*-hexaphenyl crystal.

Finally, organic nanofibers are also a nice testing ground for methods that aim to deduce directly properties of the near field such as scanning near field optical microscopy (SNOM), Fig. 1.11 [32]. To obtain the images in Fig. 1.11 an inverted epifluorescence microscope was mounted on a (x,y,z)-movable table and was used for focussed UV (360 nm) illumination of the sample outside

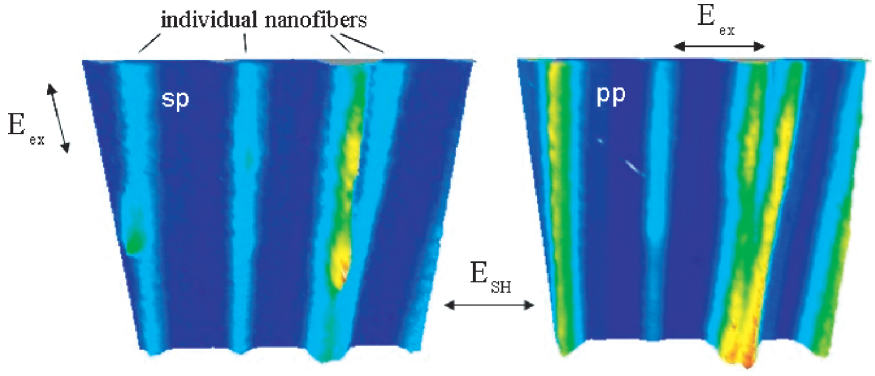

Fig. 1.10. Polarized $10 \times 10\,\mu m^2$ two-photon (400 nm) images of nanofibers on mica. The nanofibers were excited with a femtosecond laser at 780 nm with a total power of 25 mW and with its electric field vector directed as shown with respect to the nanofiber axes. The detection was always polarized parallel to the individual molecules [31]

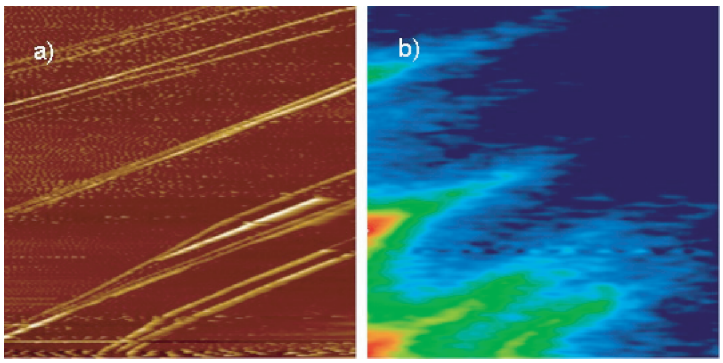

Fig. 1.11. Near field images ($45 \times 45\,\mu m^2$) of waveguiding nanofibers on mica. (**a**) Topographical image, (**b**) optical image in the near field at contact with the nanofibers. The nanofibers have been excited with UV light on the left-hand side outside the viewing area shown in the plots. They are not visible in the optical far field [32]

the direct viewing area of the SNOM. That way waveguiding through the nanofibers could be measured. It is to be noted that the low transfer rate of 425 nm photons from the luminescing nanofibers via the 160 nm diameter SNOM tip to the detector of less than 10^{-6} made rather dense needle arrays and strong focussing of the exciting UV light necessary. This, in turn, resulted in photobleaching of the samples, which limited the possible data integration time and thus the signal-to-noise ratio.

A $45 \times 45\,\mu m^2$ scan along the sample at a constant distance of a few nanometers maintained by shear force feedback is shown in Fig. 1.11, both as topographic image (Fig. 1.11a, from the shear force feedback) and as optical image (Fig. 1.11b, from the measured counts in the photomultiplier). First of all, it is interesting to note that the optical image shows some structures at all since the observation point of the SNOM is *outside* the illumination area by the excitation light. This can only be explained by waveguiding of light through the nanofibers, which then is transferred within the near field into the SNOM. Second, individual nanofibers show quite different brightnesses, although they look topographically very similar and the far field images reveal indeed almost the same brightness (not shown here). Again, since the UV excitation of the nanofibers occurs outside the viewing area of the SNOM one could argue that some nanofibers are not visible in the SNOM since they do not guide blue light of 425 nm. Measurements and calculations for waveguiding in individual nanofibers indeed have shown that the critical minimum width for waveguiding is about 220 nm [33, 34]. The waveguiding is damped mainly by reabsorption in the nanofibers. If one measures the scattered intensity as a function of distance from the excitation point, then one obtains the imaginary part of the dielectric function of an individual nanoaggregate, which is an important quantity since it determines the light-matter interaction [33].

One should also recall that the SNOM images result from a coupling between waveguiding modes in the nanofiber and waveguiding modes in the SNOM fiber. The SNOM tip acts as a scatterer which transforms the wave vector of the nanofiber mode into different wave vectors of scattered waves. Some of those scattered waves can be coupled to the propagating fiber modes. This process is most effective if there is a phase matching between the waves. Therefore, it depends on the mutual position between nanofiber and the SNOM tip. The nanofibers for which this condition accidentally is fulfilled are seen as more bright. It is tempting to assume that both waveguiding efficiency and phase matching are responsible for the strong selectivity of the SNOM.

1.5 Summary and Outlook: Future Devices From Organic Nanofibers

In this chapter growth and growth control of quasi single crystalline, fiber-like organic nanoaggregates on specific template surfaces have been discussed. By now it has thoroughly been demonstrated that organic molecular beam epitaxy of polarizable, rod-like molecules with large delocalized π-electrons (viz., *para*-phenylenes) on single crystalline, flat substrate surfaces with large electric dipole domains (viz., muscovite mica) leads to the well organized growth of organic nanofibers with remarkable optical properties. These nanofibers have been used within the last five years for a series of benchmark experiments on static and dynamic, linear and nonlinear optics as well as morphology in the mesoscopic size regime. A few applications are detailed in this chapter.

The fact that *para*-phenylenes plus muscovite mica constitute an unique combination from a crystallographic and growth dynamic point of view has resulted in unique nanoaggregates but obviously also limits the potential range of applications of these nanofibers. However, two recent developments have opened the door to a much wider application potential of organic nanofibers: (1) the possibility to transfer the nanofibers from the original growth substrate to any other substrate or into liquids [35]; and (2) the possibility to functionalize a *para*-quaterphenylene block with specific groups and the generation of aligned nanofibers from these functionalized molecules [36]. In terms of implementation of nanoaggregates into working devices the former development (1) has enabled electrical conductivity [37] as well as mechanical deformation measurements [38] on single nanofibers, whereas development (2) resulted in the growth of tailored nanoscaled frequency doubling elements [30]. Further device development thus seems to be well in reach in the nearest future [39].

Acknowledgments

The author is indebted to the Danish Research Agencies FNU and FTP and to the TMR program FASTNet of the European Community as well as the Danish National Advanced Technology Foundation for financial support. He would like to acknowledge Frank Balzer, Humboldt-University, Berlin as the coinventor of the organic *p*-6P nanofibers. Although many more people are involved in various aspects of organic nanofiber research this article is based primarily on work performed together with Jonas Beerman, Jonathan Brewer, Vladimir G. Bordo, Sergey I. Bozhevolnyi, Manuela Schiek, and Valentyn Volkov.

References

1. U. Kreibig, in *Optics of Nanosized Metals*, ed. by R.E. Hummel, P. Wißmann, Handbook of Optical Properties, Vol. II, Optics of Small Particles, Interfaces and Surfaces, (CRC, Boca Raton, 1997), p. 145
2. B.J. Butkus, Biophoton. Int. **5**, 34 (2004)
3. J. Joannopoulos, R. Meade, J. Winn, *Photonic Crystals* (Princeton Press, Princeton NJ, 1995)
4. See, e.g. the website of the company 'crystal fibre': www.**crystal-fibre**.com/
5. G. Witte, Ch. Woell, J. Mater. Res. **19**, 1889 (2004)
6. G. Ziegler, in *Thin Film Properties of Oligothiophenes*, ed. by H.S. Nalwa, Handbook of Organic Conductive Molecules and Polymers: Vol. 3. Conductive Polymers: Spectroscopy and Physical Properties, (Wiley, New York 1997)
7. B. Krause, A.C. Dürr, K.A. Ritley, H. Dosch, D. Smilgies, Phys. Rev. B **66**, 235404 (2002)
8. M. Brinkmann, S. Graff, C. Straupe, J.C. Wittmann, C. Chaumont, F. Nuesch, A. Aziz, M. Schaer, L. Zuppiroli, J. Phys. Chem. B **107**, 10531 (2003)
9. R. Resel, Thin Solid Films **433**, 1 (2003)
10. G.I. Distler, Kristall und Technik **5**, 73 (1970)
11. E. Zoyer et al., Phys. Rev. B **61**, 16538 (2000)
12. L. Athouel, G. Froyer, M.T. Riou, Synth. Met. **55–57**, 4734 (1993)
13. L. Athouel, G. Froyer, M.T. Riou, M. Schott, Thin Solid Films **274**, 35 (1996)
14. M. Era, T. Tsutsui, S. Saito, Appl. Phys. Lett. **67**, 2436 (1995)
15. F. Meghdadi, S. Tasch, B. Winkler, W. Fischer, F. Stelzer, G. Leising, Synth. Met. **85**, 1441 (1997)
16. K. Erlacher, R. Resel, J. Keckes, G. Leising, Mat. Sci. For., **321–324**, 1086 (2000)
17. M. Ichikawa, H. Yanagi, Y. Shimizu, S. Hotta, N. Suganuma, T. Koyama, Y. Taniguchi, Adv. Mat. **14**, 1272 (2002)
18. F. Quochi et al., Appl. Phys. Lett. **84**, 4454 (2004)
19. H. Yanagi, S. Okamoto, T. Mikami, Synth. Met. **91**, 91 (1997)
20. A. Niko, F. Meghdadi, C. Ambrosch-Draxl, P. Vogl, G. Leising, Synth. Met. **76**, 177 (1996)
21. F. Balzer, H.-G. Rubahn, Surf. Sci. **548**, 170 (2004)

22. F. Balzer, J. Beermann, S. Bozhevolnyi, A.C. Simonsen, H.-G. Rubahn, Nano Lett. **3**, 1311 (2003)
23. G. Koller et al., Adv. Mat. **16**, 2159 (2004)
24. A. Andreev et al., Adv. Mat. **12**, 629 (2000); Thin Solid Films **403–404**, 444 (2002)
25. F. Balzer, H.-G. Rubahn, Appl. Phys. Lett. **79**, 3860 (2001); Surf. Sci. **507–510**, 588 (2002); Adv. Funct. Mat. **15**, 17 (2005)
26. F. Balzer, H.-G. Rubahn, Nano Lett. **2**, 747 (2002)
27. F. Balzer, L. Kankate, H. Niehus, R. Frese, C. Maibohm, H.-G. Rubahn, Nanotechnology **17**, 984 (2006)
28. A.C. Simonsen, H.-G. Rubahn, Nano Lett. **2**, 1379 (2002)
29. F. Balzer, K. Al-Shamery, R. Neuendorf, H.-G. Rubahn, Chem. Phys. Lett. **368**, 307 (2003)
30. J. Brewer, M. Schiek, A. Luetzen, K. Al-Shamery, H.-G. Rubahn, Nano Lett. **6**, 2656 (2006)
31. J. Beermann, S.I. Bozhevolnyi, V.G. Bordo, H.-G. Rubahn, Opt. Comm. **237**, 423 (2004)
32. V.S. Volkov, S.I. Bozhevolnyi, V.G. Bordo, H.-G. Rubahn, J. Microsc. **215**, 241 (2004)
33. F. Balzer, V.G. Bordo, A.C. Simonsen, H.-G. Rubahn, Appl. Phys. Lett. **82**, 10 (2003)
34. F. Balzer, V.G. Bordo, A.C. Simonsen, H.-G. Rubahn, Phys. Rev. B **67**, 115408 (2003)
35. J. Brewer, C. Maibohm, L. Jozefowski, L. Bagatolli, H.-G. Rubahn, Nanotechnology **16**, 2396 (2005)
36. M. Schiek, A. Luetzen, R. Koch, K. Al-Shamery, F. Balzer, R. Frese, H.-G. Rubahn, Appl. Phys. Lett. **86**, 153107 (2005)
37. J. Kjelstrup-Hansen, H.H. Henrichsen, P. Boggild, H.-G. Rubahn, Thin Solid Films **515**, 827 (2006)
38. J. Kjelstrup-Hansen, P. Bogild, H.-G. Rubahn, Small **2**, 660 (2006)
39. K. Al-Shamery, H.-G. Rubahn, H. Sitter (ed.), New organic nanostructures for next generation devices. Springer Ser. Mater. Sci., Berlin (2007)

http://www.springer.com/978-3-540-72674-6

Self-Organized Morphology in Nanostructured Materials
Al-Shamery, K.; Parisi, J. (Eds.)
2008, XIII, 176 p., Hardcover
ISBN: 978-3-540-72674-6